Eur. Phys. J. A **22**, 355–362 (2004)
DOI 10.1140/epja/i2004-10046-4

THE EUROPEAN PHYSICAL JOURNAL A

Magic gaps and intruder levels in triaxially superdeformed nuclei

R. Bengtsson[1] and H. Ryde[2,a]

[1] Department of Mathematical Physics, Lund Institute of Technology, Box 118, S-221 00 Lund, Sweden
[2] Department Physics, University of Lund, Box 118, S-221 00 Lund, Sweden

Received: 28 April 2004 /
Published online: 11 November 2004 –
Communicated by A. Molinari

Abstract. Nuclear shell model calculations based on a modified harmonic-oscillator potential result in amazingly stable triaxial nuclear shapes. Major gaps in the single-particle energy spectra at proton number 71 and neutron number 94 combine constructively at low and intermediate rotational frequencies. At high frequencies, gaps at proton number 72 and neutron number 97 combine in an equally favourable way. The sizes of the gaps may be as large as 35% of the values for the gaps at the classical magic numbers 50 and 82 at spherical shape. The dependence on the positions of the intruder levels in forming the gaps is discussed. Experimentally observed rotational bands in lutetium ($Z = 71$) and hafnium ($Z = 72$) appear in isotopes and frequency ranges, which are consistent with the gaps in the theoretical single-particle energy spectra.

PACS. 21.10.-k Properties of nuclei; nuclear energy levels

1 Introduction

The shapes, and particularly the shape changes, of any physical entity are of fundamental interest as they are connected to symmetry and the breaking of symmetry. In systems with spherical symmetry the energy levels show a high degree of degeneracy. Bunches of degenerate levels are separated by large energy gaps. In the atomic nucleus such gaps appear, for example, at neutron numbers 50, 82 and 126, which for historical reasons are often referred to as magic numbers. However, most of the known nuclei are non-spherical, having a prolate quadrupole deformation with rotational symmetry, that is, the two minor axes have the same length. The symmetry properties of such nuclei are enhanced for certain simple axis ratios, such as 2 : 1, that is, the longer axis is twice as long as the two shorter axes. The second minimum in the fission barrier corresponds to this axis ratio, as does the shape of many superdeformed nuclei observed at high angular momentum [1]. Breaking the rotational symmetry results in triaxially deformed nuclei, in which the three axes have different lengths. It is not expected that such nuclei should show pronounced shell effects, *e.g.* a bunching of energy levels strong enough to produce minima in the total energy of the nucleus at large quadrupole deformation. However, such energy minima have been found.

[a] e-mail: hans.ryde@nuclear.lu.se

2 Experimental observations

The first case of shape coexistence in heavy nuclei involving triaxial shapes at large quadrupole deformation was reported a few years ago in the nucleus ^{163}Lu [2]. Transition quadrupole moments almost twice as large as the normal ones were observed in one rotational band, which was interpreted as being built on the proton $i_{13/2}$ intruder configuration.

Several triaxially superdeformed (TSD) bands have then been observed in many lutetium nuclei. Thus, a TSD band was reported in ^{165}Lu [3] and the triaxial superdeformation in ^{163}Lu was confirmed [4] and the band extended to spin 97/2 $\hbar$ in ref. [5]. The deduction of large average transition quadrupole moments, from lifetime measurements, for a series of lutetium isotopes, ^{163}Lu, ^{164}Lu and ^{165}Lu, resulted in values about twice as large as that for normally deformed bands [6,7]. Furthermore, from a fluctuation analysis [8] of the ridge yields in $E_\gamma - E_\gamma$ spectra, it can be concluded that there is a separate triaxial potential well at a different deformation, coexisting with a normally deformed potential well.

There are thus many indications of triaxial nuclear shapes with more than 30 cases now known. A direct consequence of a rotational motion of a triaxial body would be a wobbling mode, the classical analogue of which is the spinning motion of an asymmetric top. The nuclear wobbling mode was predicted by Bohr and Mottelson [9] and has recently been discussed in several papers [10–12]. This is now a very active field of research and several

papers reporting evidence for wobbling phonon excitations in ^{163}Lu have been published [5,13–15].

Further evidence for triaxial superdeformation has been reported in other lutetium nuclei such as in ^{161}Lu and ^{162}Lu [16] as well as in ^{165}Lu [17,18] and ^{167}Lu [19,20]. Triaxial superdeformation was also seen in the odd-odd nucleus ^{164}Lu [21].

Furthermore, evidence for triaxially superdeformed rotational bands was found in even-even hafnium isotopes, namely, ^{168}Hf [22], ^{170}Hf [23] and ^{174}Hf [24]. However, it should be noted that no indications of triaxially deformed bands were found in either ^{166}Hf [25] or in ^{169}Hf [26] in spite of considerable effort. On the other hand, triaxially superdeformed bands were also found in other mass regions.

3 Theoretical investigations

The first rotational band belonging to the family of bands, which later were to be referred to as triaxial superdeformed (TSD) rotational bands, was reported in ^{163}Lu by Schmitz *et al.* [27]. It was interpreted as a proton $i_{13/2}$ rotational band with large deformation, which was suggested to be associated with an energy minimum in a total Routhian surface (TRS), calculated for the $[660]1/2^+$ configuration at a low rotational frequency $\hbar\omega = 0.20$ MeV. The energy minimum appears at a nearly prolate shape with $\beta = 0.33$.

In a subsequent paper, Schmitz *et al.* [2] report measured transitional quadrupole moments for the previously observed [27] $i_{13/2}$ band in ^{163}Lu. The large average value of the quadrupole moment (10.7 b) suggests an even larger deformation than reported in ref. [27]. The TRS calculations were therefore extended to larger deformations, and two pronounced energy minima were found at $\beta = 0.37$ and $\gamma = \pm 14°$. Calculated quadrupole moments at these deformations are, within the expected accuracy, in good agreement with the experimental transition quadrupole moment.

The notation "triaxial superdeformed" bands can be traced back to a paper by Schnack-Petersen *et al.* [3] of 1995. The paper contains the first, and so far only, detailed theoretical investigation of the properties of TSD rotational bands. Total energy surfaces (TES) [28] were calculated for several configurations in the $Z = 71$ isotopes ^{163}Lu and ^{165}Lu with 92 and 94 neutrons, respectively. It was observed that well-developed TSD energy minima appeared in nearly all low-lying configurations in the two nuclei. It was therefore concluded that TSD energy minima could not be associated with any specific configuration, but had to be the result of an important, so far unnoticed, shell structure at TSD shapes.

In order to understand the shell structure, Schnack-Petersen *et al.* [3] calculated single-particle energy levels at zero rotational frequency as a function of the deformation from spherical to TSD shapes. It was then evident that a major gap appeared at TSD shapes for neutron number 94. In the proton system, a smaller gap appeared at proton number 70, but a pair of highly alignable $i_{13/2}$ levels

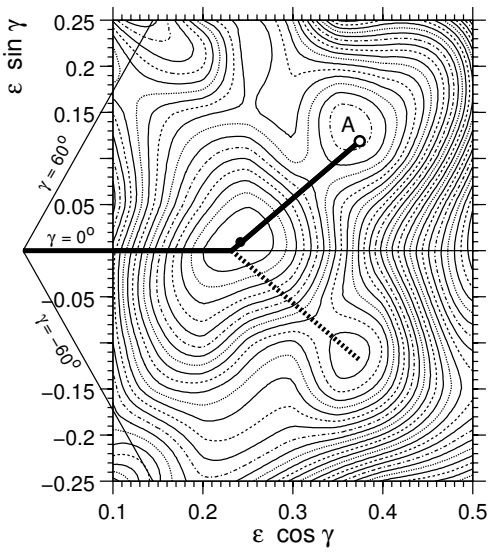

Fig. 1. The total energy surface for ^{165}Lu, with $Z = 71$ and $N = 94$, is shown at a spin value of $73/2\hbar$. It is calculated for the lowest configuration with positive parity for both protons and neutrons and signature $\alpha = 1/2$ for protons and $\alpha = 0$ for neutrons. The paths through the deformation plane used for calculating the single-particle levels in figs. 3 and 4 are shown, as are the outlines for $\gamma = 0°$and $\pm 60°$. At the point marked A, single-particle levels have been calculated as a function of the rotational frequency. They are shown in figs. 3 and 4. The contour line separation is 0.20 MeV.

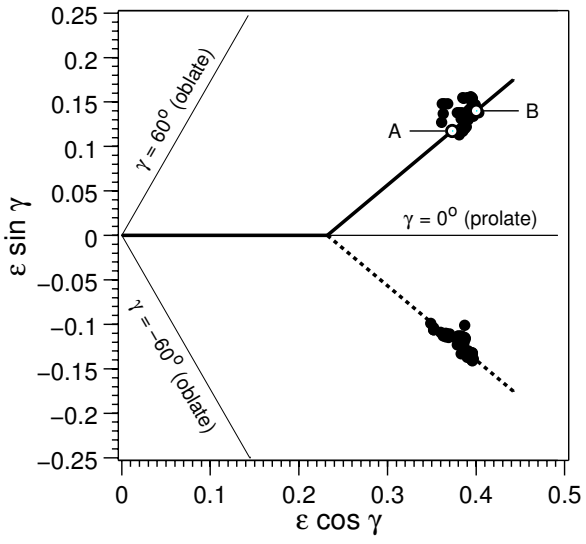

Fig. 2. Systematics of TSD energy minima in the vacuum configuration (positive parity and signature zero for both protons and neutrons) of the hafnium isotopes with neutron numbers 92, 94 and 96. The points marked A and B show the deformations at which single-particle levels have been calculated as a function of the rotational frequency in figs. 3 and 4 (A) and in figs. 5 and 6 (B).

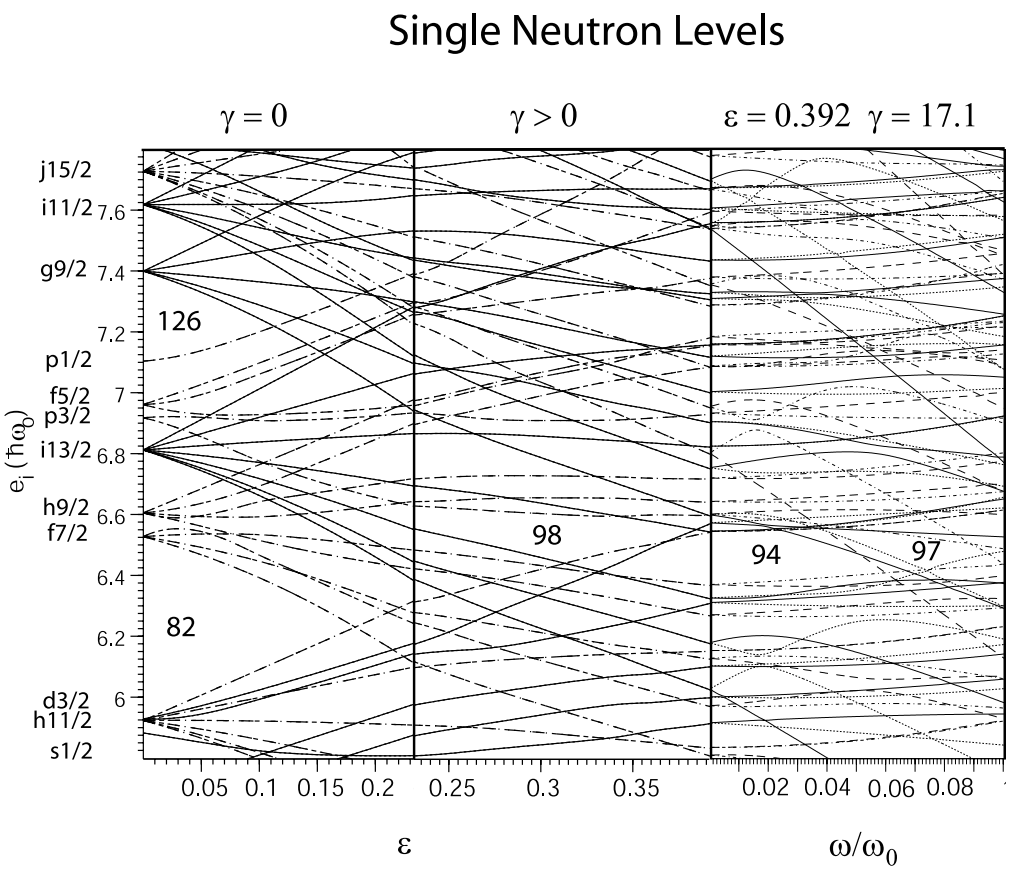

Fig. 3. Single-neutron levels calculated along the path (solid line) shown in fig. 1 from spherical shape to a TSD shape at $\gamma = +17.1^\circ$ and $\varepsilon = 0.392$. The three sections of the triptych refer i) to the increase in the quadrupole deformation only, ii) to the path out in the γ-plane and finally iii) to the increase of the rotational frequency. The energy scale and the rotational frequency are given in units of the oscillator frequency ω_0, which makes the scales on the axes independent of the particle number. For ^{166}Hf, the oscillator frequency for neutrons is $\hbar\omega_0 = 7.933$ MeV at the TSD shape. The spherical subshell notations for $\varepsilon = 0$ are shown for the pertinent levels.

immediately above the gap were assumed to penetrate the gap already at low rotational frequencies, shifting the gap to proton number 72 at higher rotational frequencies.

The observation that $N = 94$ and $Z = 72$ were likely to appear as significant gaps in the single-particle spectra for rotational frequencies, at which TSD bands had been observed, identified ^{166}Hf as the central nucleus in a region of nuclei with predicted TSD states. However, subsequent experimental data only partially confirmed the predictions. TSD states are apparently much more favoured in the Lu isotopes than in the Hf isotopes, and so far no TSD states have been observed in the supposedly most favourable nucleus ^{166}Hf [25].

The above discrepancies have stimulated us to investigate the underlying nuclear structure and the reasons for the specific properties of high-spinning nuclei with proton numbers 71 and 72 and neutron numbers close to 94.

4 Energy minima at TSD shapes

Calculated total energy surfaces (TES), like the one in fig. 1, provide a straightforward way of finding triaxially superdeformed energy minima. TES have been calculated using the cranked, modified oscillator model [29] with model parameters and computational specifications as described in ref. [28]. TSD energy minima appear in the TES from spin below $10\hbar$ in some nuclei all the way up to spin $50\hbar$ and higher. Several examples of total energy surfaces can be found in papers reporting experimental observations: ^{161}Lu in ref. [16], ^{162}Lu in ref. [16], ^{163}Lu in refs. [3,4,6,15], ^{164}Lu in refs. [6,21], ^{165}Lu in refs. [3,17], ^{167}Lu in ref. [20] and ^{168}Hf in ref. [22].

It should be noted that the relatively shallow TSD minima correspond to well-defined, well-localized nuclear states, due to their special structure, which involves the occupation of unique intruder levels [30].

TSD states appear in two narrow regions in deformation space, centred around $\varepsilon \approx 0.40$ and $\gamma \approx \pm 20^\circ$. This is illustrated in fig. 2 which shows the location of TSD energy minima in the hafnium isotopes ^{164}Hf, ^{166}Hf and ^{168}Hf. Based on calculations for about fifteen nuclei in the vicinity of ^{166}Hf, we have determined the centroid of the TSD region, considering both energy minima with positive and negative values of γ. We have then constructed a

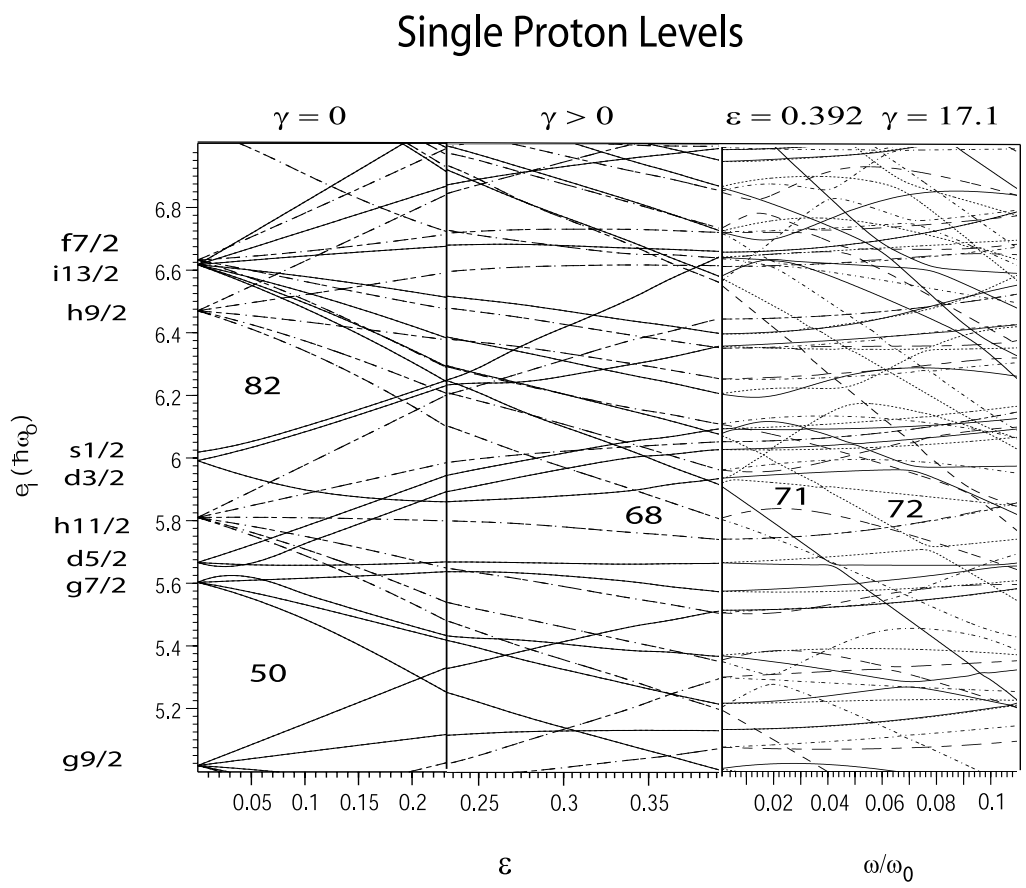

Fig. 4. Single-proton levels calculated along the path towards the TSD shape at $\gamma = +17.1°$ and $\varepsilon = 0.392$. The triptych is analogous to the one in fig. 3. For protons the oscillator frequency has the value $\hbar\omega_0 = 7.262$ MeV for ^{166}Hf at the TSD shape.

path in deformation space from spherical to TSD shapes (cf. figs. 1 and 2). The path starts to deviate from the rotation symmetric quadrupole shapes ($\gamma = 0°$) at an ε-value of 0.232, which is a representative deformation for normally deformed rotational bands in the nuclei considered, cf. fig. 1. From this point, the path follows a straight line through the (ε, γ)-plane, passing through the points ($\varepsilon = 0.392,\ \gamma = 17.1°$) and ($\varepsilon = 0.424,\ \gamma = 19.3°$). The first point, marked A in figs. 1 and 2, represents a typical TSD shape in ^{163}Lu and ^{165}Lu, while the second point, marked B in fig. 2, represents a shape that is more typical for hafnium isotopes with a neutron number below 100. The hexadecapole deformation, ε_4, is kept at zero when $\gamma = 0$, *i.e.* for $\varepsilon \leq 0.232$. From that point, ε_4 increases linearly with $\varepsilon \cos\gamma$ along the path through the (ε, γ)-plane, reaching the value $\varepsilon_4 = 0.051$ when $\varepsilon \cos\gamma = 0.5$.

Single-particle levels calculated for negative γ-values along the dotted path in figs. 1 and 2 are identical to those along the path for positive γ-values (solid line). However, the levels respond differently to rotation.

At high spin, the energy minima with $\gamma > 0°$ are always energetically favoured compared to those with $\gamma < 0°$. Only at low spin, when the TSD bands lie high above the yrast line, may energy minima with $\gamma < 0°$ have a lower energy than corresponding minima with $\gamma > 0°$. They are then not likely to be observed experimentally. We have therefore restricted the present investigation to TSD shapes with $\gamma > 0°$.

At two points, marked A and B in fig. 2, we have cranked the nucleus about its shortest axis (corresponding to $\gamma > 0°$) up to high rotational frequencies. In the next two sections the influence of this rotation on the single-particle levels is discussed. The results for negative γ-values are not discussed, but will be treated in a forthcoming publication [31].

5 Single-particle level structure at TSD shape in ^{163}Lu and ^{165}Lu

The appropriate single-particle energy diagrams for the lutetium isotopes ^{163}Lu and ^{165}Lu are shown in figs. 3 (neutrons) and 4 (protons). Each figure consists of three sections. The left section shows the single-particle levels at prolate shape ($\gamma = 0°$) from spherical ($\varepsilon = 0$) to $\varepsilon = 0.232$, which is very close to the deformation of the normally deformed bands in the two Lu isotopes. The middle section of the figures shows the single-particle levels along the path through the (ε, γ)-plane specified in sect. 4. This path is also shown in figs. 1 and 2.

At TSD shapes, the gap at neutron number 94 is very large (in fig. 3 about 35% of the spherical $N = 82$

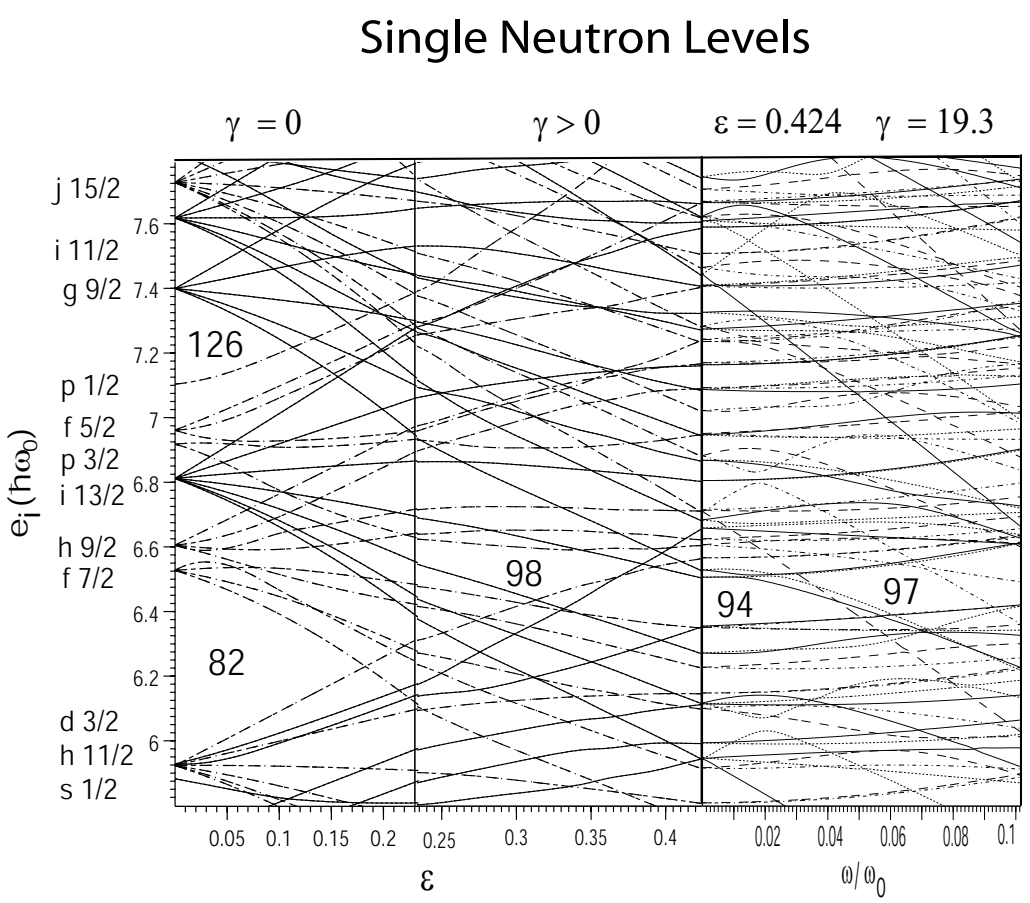

Fig. 5. Single-neutron levels calculated along the deformation path towards the more deformed TSD shape at $\varepsilon = 0.424$ and $\gamma = +19.3^\circ$ (point B in fig. 2), where the rotation is introduced. The three sections of the triptych are analogous to those in fig. 3. At the TSD shape, $\hbar\omega_0 = 7.954$ MeV for neutrons in ^{166}Hf.

gap) at rotational frequencies up to about $\omega/\omega_0 = 0.03$ ($\hbar\omega \approx 0.24$ MeV).

It lies entirely embedded in levels from the $N = 4$, $N = 5$ and $i_{13/2}$ oscillator shells. The position of these levels is experimentally confirmed at the ground-state deformation ($\varepsilon \approx 0.25$). The prediction of a sizable $N = 94$ gap should therefore be reliable and the existence of this gap most certainly plays an important role for the appearance of TSD states. The gap is made possible by the large splitting of the levels originating from the $d_{3/2}$ subshell as the γ-deformation increases.

At higher rotational frequencies, the $N = 94$ gap is penetrated by highly alignable intruder levels from above (one $j_{15/2}$ level and two levels originating from the $g_{9/2}$ subshell but with mixed wave functions, dominated by $i_{11/2}$ components). At $\omega/\omega_0 \approx 0.065$ ($\hbar\omega \approx 0.52$ MeV), the gap is completely closed. The position of the intruder levels is not very well known. It is therefore nearly impossible to predict at which angular momentum the gap will close. Note that above the gap closure, at frequencies near $\omega/\omega_0 = 0.075$, a moderately sized gap opens up at neutron number 97.

Contrary to previous claims, the proton levels (fig. 4) do not show a major gap at $Z = 72$, nor at any other neighbouring proton number, such as 71, which corresponds to the experimentally favoured Lu isotopes. However, the level density in the rotational, single-proton spectrum is relatively low for proton numbers between 70 and 73, resulting in the shell-correction energy being generally favourable.

Actually, the proton spectrum is more similar to the neutron spectrum than it may appear at first glance. If we disregard the intruder levels from the $h_{9/2}$ and $i_{13/2}$ subshells, there is a substantial gap (35% of the spherical gap at $Z = 50$) between the fourth level (from below) of the $h_{11/2}$ subshell and the lowest level of the $d_{3/2}$ subshell at TSD shapes. The gap is embedded in levels with experimentally confirmed positions from the $N = 4$ and $h_{11/2}$ oscillator shells. It should therefore be as reliable as the neutron gap at $N = 94$. With no intruder levels, the magic number would be $Z = 68$. However, the calculations predict that two intruder levels from the $h_{9/2}$ subshell and two intruder levels from the $i_{13/2}$ subshell will fall inside the gap. The exact position of these intruder levels is not known, preventing a firm prediction of a most favourable proton number. Thus, it can be observed that shifting the intruder levels just a few hundred keV can make any proton number between 68 and 72 the most favourable one. For example, lowering the $h_{9/2}$ subshell by 500 keV, leaving the other levels unchanged, will

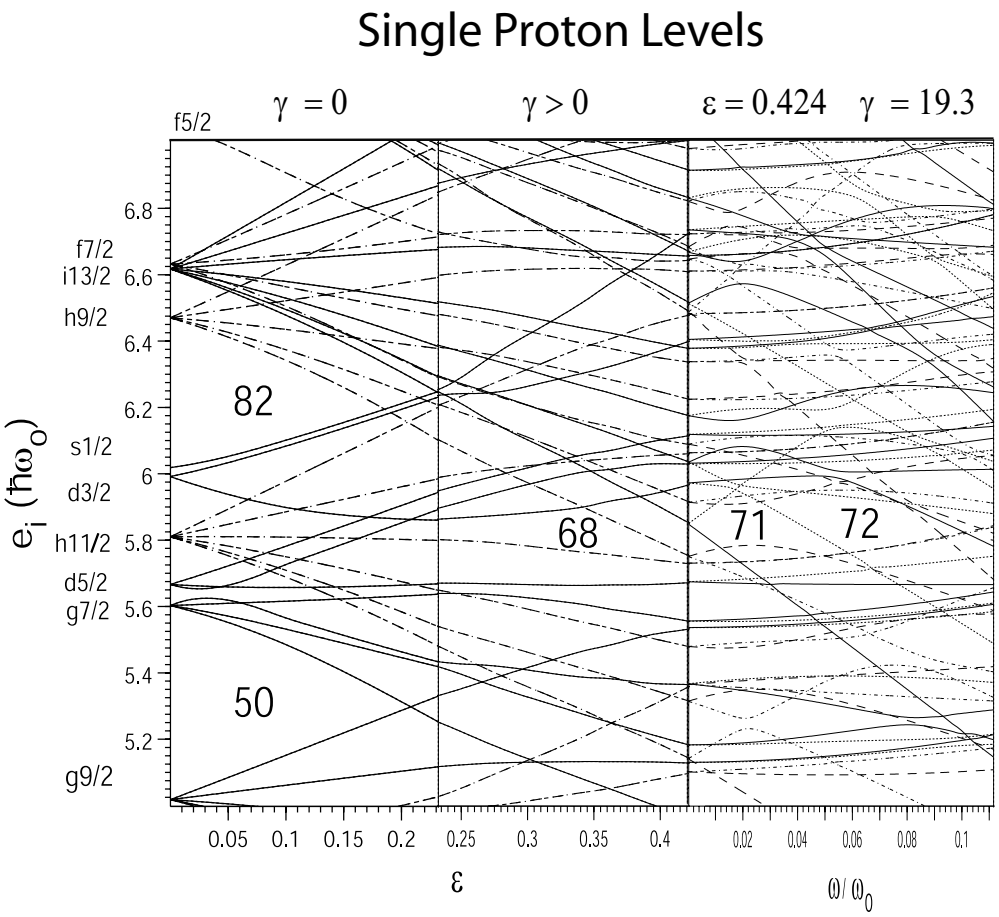

Fig. 6. Single-proton levels calculated along the same path as in fig. 5. The three sections of the triptych are analogous to those in fig. 3. The value of $\hbar\omega_0$ is 7.281 MeV for protons in ^{166}Hf at the TSD shape.

make the gap at $Z = 71$ very big, without changing the size of the gap at $Z = 72$.

6 Single-particle level structure at TSD shape in even-even nuclei near ^{166}Hf

The intruder levels are strongly deformation driving. Calculated TSD shapes will therefore depend on which intruder levels are occupied. They thus depend both on the nucleus and on the configuration. Thus, in the lowest-lying configuration in the hafnium isotopes a second $i_{13/2}$ intruder level is occupied. As a result, the TSD energy minima appear at a slightly larger deformation than in the lutetium isotopes. This is illustrated in fig. 2, where each TSD minimum of the lowest-lying configuration in the hafnium isotopes ^{164}Hf, ^{166}Hf and ^{168}Hf is represented by a black dot. All energy minima found for $I \leq 50\hbar$ are included, in total 43 minima with $\gamma > 0°$ and 37 minima with $\gamma < 0°$. Almost all of the minima with $\gamma > 0°$ have a larger deformation than the representative deformation (point A) for the lutetium isotopes and most of them cluster close to point B.

Rotational single-particle levels, calculated at the larger deformation $\varepsilon = 0.424$ and $\gamma = 19.3°$(point B in fig. 2) are shown in figs. 5 and 6. Compared to the corresponding figs. 3 and 4, a few important differences can be found. The moderate gaps, which at the smaller deformation appeared at high frequencies for proton number 72 and neutron number 97, have at the larger deformation developed into major gaps. At the same time, the neutron gap at $N = 94$ has decreased in size and there is no energy gap at all for $Z = 72$ at low frequencies. This implies that the most favoured neutron number for hafnium is 97 and not 94 as previously claimed. It also implies that the favoured TSD states in hafnium should appear at high rotational frequencies. The neutron gap at $N = 97$ (fig. 5) extends over the frequency range $0.03 < \omega/\omega_0 < 0.09$ and the proton gap at $Z = 72$ (fig. 6) over approximately the same range in ω/ω_0. Combining the two gaps will result in favoured TSD states in the frequency range $0.3\,\text{MeV} < \hbar\omega < 0.6\,\text{MeV}$. It should be observed that the three intruder levels separating the gaps at $N = 94$ and $N = 97$ in fig. 5 slope steeply upwards with decreasing frequency. TSD bands in isotopes with more than 94 neutrons will therefore not be energetically favoured at low rotational frequencies. This effect will be further strengthened in the hafnium isotopes due to the $i_{13/2}$ level separating the proton gaps at $Z = 71$ and $Z = 72$ in fig. 6. As a result, the lowest spin, which

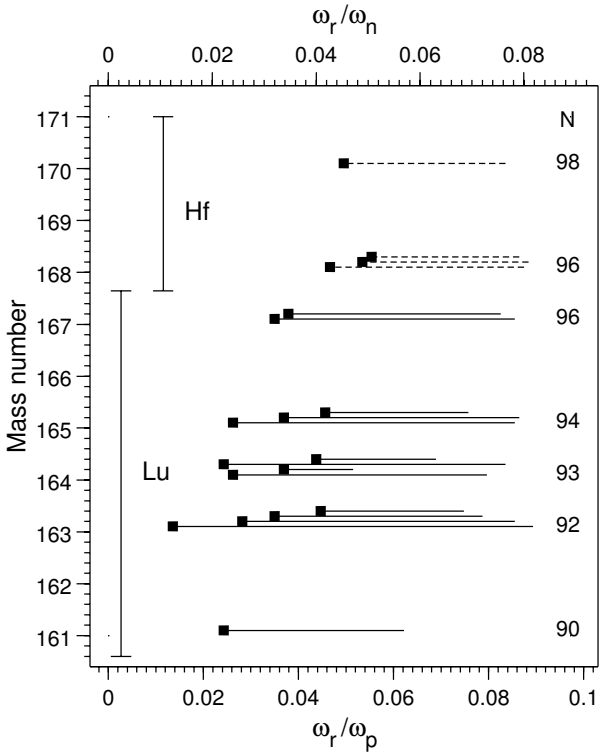

Fig. 7. Frequency ranges for experimentally observed TSD bands. The frequency for the lowest transition in a band is shown by a square from which a line extends up to the frequency of the highest observed transition in that band. Solid lines are used for lutetium and dashed lines for hafnium. The neutron number is indicated to the right. When several bands are observed in a nucleus, the band denoted TSD1 in the experimental papers corresponds to the lowest line. The next higher line corresponds to TSD2 and so on. To simplify the comparison with the theoretical single-particle diagrams, the experimental rotational frequency, ω_r, has been divided by the oscillator frequency for protons (lower scale) and neutrons (upper scale). The oscillator frequencies given in figs. 3 and 4 have been used.

has a TSD energy minimum, is higher in hafnium than in lutetium and increases with increasing neutron number.

7 Comparisons with experiment

It can be concluded from the two previous sections that proton number 71 (lutetium) will combine optimally with neutron number 94 at low and intermediate rotational frequencies, whereas proton number 72 (hafnium) will combine optimally with neutron number 97 at higher rotational frequencies and a slightly larger deformation. It can therefore be expected that TSD bands should be observed down to relatively low rotational frequencies in lutetium, in particular in isotopes with 94 or fewer neutrons. In hafnium, TSD bands are expected to be observed only at higher rotational frequencies and preferentially in isotopes with neutron numbers close to 97.

The frequency intervals in which TSD bands have been experimentally observed in the Lu and Hf isotopes are shown in fig. 7. In the Hf isotopes ($N = 96$ and 98), the bands stop near the frequency $\omega_r/\omega_p = 0.05$, whereas in the Lu isotopes with $N \leq 94$, TSD bands have been observed down to frequencies below $\omega_r/\omega_p = 0.03$. However, in ^{167}Lu with $N = 96$, both observed bands actually do stop above $\omega_r/\omega_p = 0.03$. This is also the case for some of the excited TSD bands in the lighter Lu isotopes. In these bands, nucleons can be excited to levels above the gaps at $N = 94$ and/or $Z = 71$, which makes the excitation energy high and the bands hard to observe at low rotational frequencies. It is therefore not surprising that such excited bands are observed in essentially the same frequency interval as the TSD bands in the heavier Hf isotopes.

8 Conclusions

The experimental data available so far are surprisingly consistent with theoretical predictions about the frequency range in which TSD bands are most likely to be observed in a number of Lu and Hf isotopes. This gives some reliability to the major gaps appearing in the single-particle energy spectra at TSD shapes. However, the precise size and extension of these gaps are critically sensitive to the exact position of a handful of intruder levels from higher shells which penetrate the gaps. In cases when TSD bands are experimentally linked to bands at normal deformation and thus the excitation energy is known, a comparison with calculated total energies for the TSD bands shows discrepancies which cannot be neglected [5]. One possible explanation is that the position of the intruder levels and, as a consequence, the magnitude of the magic gaps at TSD shapes are not fully correct. The discrepancies may also indicate the presence of wobbling [5] or tilted rotation [32]. Continued experimental and theoretical investigations are needed in order to solve this problem.

References

1. P.J. Twin, B.M. Nyakó, A.H. Nelson, J. Simpson, M.A. Bentley, H.W. Cranmer-Gordon, P.D. Forsyth, D. Howe, A.R. Mokhtar, J.D. Morrison, J.F. Scharpey-Schafer, G. Sletten, Phys. Rev. Lett. **57**, 811 (1986).
2. W. Schmitz, H. Hübel, C.X. Yang, G. Baldsiefen, U. Birkental, G. Frölingsdorf, D. Metha, R. Müsseler, M. Neffgen, P. Willsau, J. Gascon, G.B. Hagemann, A. Maj, D. Müller, J. Nyberg, M. Piiparinen, A. Virtanen, R. Wyss, Phys. Lett. B **303**, 230 (1993).
3. H. Schnack-Petersen, R. Bengtsson, R.A. Bark, P. Bosetti, A. Brockstedt, H. Carlsson, L.P. Ekström, G.B. Hagemann, B. Herskind, F. Ingebretsen, H.J. Jensen, S. Leoni, A. Nordlund, H. Ryde, P.O. Tjøm, C.X. Yang, Nucl. Phys. A **594**, 175 (1995).
4. J. Domscheit, S. Törmänen, B. Aengenvoort, H. Hübel, R.A. Bark, M. Bergström, A. Bracco, R. Chapman, D.M. Cullen, C. Fahlander, S. Frattini, A. Görgen, G.B. Hagemann, A. Harsmann, B. Herskind, H.J. Jensen, S.L. King, S. Lenzi, D. Napoli, S.W. Ødegård, C.M. Petrache, H. Ryde, U.J. van Severen, G. Sletten, P.O. Tjøm, C. Ur, Nucl. Phys. A **660**, 381 (1999).

5. D.R. Jensen, G.B. Hagemann, I. Hamamoto, B. Herskind, G. Sletten, J.N. Wilson, S.W. Ødegård, K. Spohr, H. Hübel, P. Bringel, A. Neußer, G. Schönwaßer, A.K. Singh, W.C. Ma, H. Amro, A. Bracco, S. Leoni, G. Benzoni, A. Maj, C.M. Petrache, G. Lo Bianco, P. Bednarczyk, D. Curien, Eur. Phys. J. A **19**, 173 (2004).
6. G. Schönwaßer, H. Hübel, G.B. Hagemann, J. Domscheit, A. Görgen, B. Herskind, G. Sletten, J.N. Wilson, D.R. Napoli, C. Rossi-Alvarez, D. Bazzacco, R. Bengtsson, H. Ryde, P.O. Tjøm, S.W. Ødegård, Eur. Phys. J. A **13**, 291 (2002).
7. G. Schönwaßer, H. Hübel, G.B. Hagemann, H. Amro, R.M. Clark, M. Cromaz, R.M. Diamond, P. Fallon, B. Herskind, G. Lane, W.C. Ma, A.O. Macchiavelli, S.W. Ødegård, G. Sletten, D. Ward, J.N. Wilson, Eur. Phys. J. A **15**, 435 (2002).
8. S.W. Ødegård, B. Herskind, T. Døssing, G.B. Hagemann, D.R. Jensen, G. Sletten, J.N. Wilson, S. Leoni, P.O. Tjøm, P. Bednarczyk, D. Curien, Eur. Phys. J. A **14**, 309 (2002).
9. A. Bohr, B.R. Mottelson, *Nuclear Structure*, Vol. **II** (W.C. Benjamin, 1975).
10. I. Hamamoto, Phys. Rev. C **65**, 044305 (2002).
11. I. Hamamoto, G.B. Hagemann, Phys. Rev. C **67**, 014319 (2003).
12. M. Matsuzaki, Y.R. Shimizu, K. Matsuyanagi, Phys. Rev. C **65**, 041303 (2002).
13. S.W. Ødegård, G.B. Hagemann, D.R. Jensen, M. Bergström, B. Herskind, G. Sletten, S. Törmänen, J.N. Wilson, P.O. Tjøm, I. Hamamoto, K. Spohr, H. Hübel, A. Görgen, G. Schönwaßer, A. Bracco, S. Leoni, A. Maj, C.M. Petrache, P. Bednarczyk, D. Curien, Phys. Rev. Lett. **86**, 5866 (2001).
14. D.R. Jensen, G.B. Hagemann, I. Hamamoto, S.W. Ødegård, B. Herskind, G. Sletten, J.N. Wilson, K. Spohr, H. Hübel, P. Bringel, A. Neußer, G. Schönwaßer, A.K. Singh, W.C. Ma, H. Amro, A. Bracco, S. Leoni, G. Benzoni, A. Maj, C.M. Petrache, G. Lo Bianco, P. Bednarczyk, D. Curien, Phys. Rev. Lett. **89**, 142503 (2002).
15. D.R. Jensen, G.B. Hagemann, I. Hamamoto, S.W. Ødegård, M. Bergström, B. Herskind, G. Sletten, S. Törmänen, J.N. Wilson, P.O. Tjøm, K. Spohr, H. Hübel, A. Görgen, G. Schönwaßer, A. Bracco, S. Leoni, A. Maj, C.M. Petrache, P. Bednarczyk, D. Curien, Nucl. Phys. A **703**, 3 (2002).
16. P. Bringel, H. Hübel, H. Amro, M. Axiotis, D. Bazzacco, S. Bhattachary, R. Bhowmik, J. Domscheit, G.B. Hagemann, D.R. Jensen, Th. Kröll, S. Lunardi, D.R. Napoli, A. Neußer, S.C. Pancholi, C.M. Petrache, G. Schönwaßer, A.K. Singh, C. Ur, Eur. Phys. J. A **16**, 155 (2003).
17. G. Schönwaßer, H. Hübel, G.B. Hagemann, P. Bednarczyk, G. Benzoni, A. Bracco, P. Bringel, R. Chapman, D. Curien, J. Domscheit, B. Herskind, D.R. Jensen, S. Leoni, G. Lo Bianco, W.C. Ma, A. Maj, A. Neußer, S.W. Ødegård, C.M. Petrache, D. Roßbach, H. Ryde, K.H. Spohr, A.K. Singh, Phys. Lett. B **552**, 9 (2003).
18. G. Schönwaßer, N. Nenoff, H. Hübel, G.B. Hagemann, P. Bednarczyk, G. Benzoni, A. Bracco, P. Bringel, R. Chapman, D. Curien, J. Domscheit, B. Herskind, D.R. Jensen, S. Leoni, G. Lo Bianco, W.C. Ma, A. Maj, A. Neußer, S.W. Ødegård, C.M. Petrache, D. Roßbach, H. Ryde, A.K. Singh, K.H. Spohr, Nucl. Phys. A **375**, 393 (2004).
19. C.X. Yang, X.G. Wu, H. Zheng, X.A. Liu, Y.S. Chen, C.W. Shen, Y.J. Ma, J.B. Lu, S. Wen, G.S. Li, S.G. Li, G.J. Yuan, P.K. Weng, Y.Z. Liu, Eur. Phys. J. A **1**, 237 (1998).
20. H. Amro, W.C. Ma, R.M. Diamond, J. Domscheit, P. Fallon, A. Görgen, B. Herskind, H. Hübel, D.R. Jensen, Y. Li, A.O. Macchiavelli, D. Roux, G. Sletten, J. Thompson, D. Ward, I. Wiedenhöver, J.N. Wilson, J.A. Winger, Phys. Lett. B **553**, 197 (2003).
21. S. Törmänen, S.W. Ødegård, G.B. Hagemann, A. Harsmann, M. Bergström, R.A. Bark, B. Herskind, G. Sletten, P.O. Tjøm, A. Görgen, H. Hübel, B. Aengenvoort, U.J. van Severen, C. Fahlander, D. Napoli, S. Lenzi, C. Petrache, C. Ur, H.J. Jensen, H. Ryde, R. Bengtsson, A. Bracco, S. Frattini, R. Chapman, D.M. Cullen, S.L. King, Phys. Lett. B **454**, 8 (1999).
22. H. Amro, P.G. Varmette, W.C. Ma, B. Herskind, G.B. Hagemann, G. Sletten, R.V.F. Janssens, A. Bracco, M. Bergström, M. Carpenter, J. Domscheit, S. Frattini, D. Hartley, H. Hübel, T.L. Khoo, T. Lauritzen, K. Lister, B. Million, S.W. Ødegård, R.B. Piercey, L.L. Riedinger, K.A. Schmidt, S. Siem, J.A. Winger, Phys. Lett. B **506**, 39 (2001).
23. A. Neußer, H. Hübel, G.B. Hagemann, S. Bhattacharya, P. Bringel, D. Curien, O. Dorvaux, J. Domscheit, F. Hannachi, D.R. Jensen, A. Lopez-Martens, E. Mergel, N. Nenoff, A.K. Singh, Eur. Phys. J. A **15**, 439 (2002).
24. M.K. Djongolov, D.J. Hartley, L.L. Riedinger, F.G. Kondev, R.V.F. Janssens, K. Abu Saleem, I. Ahmad, D.L. Balabanski, M.P. Carpenter, P. Chowdhury, D.M. Cullen, M. Danchev, G.D. Dracoulis, H. El-Masri, J. Goon, A. Heinz, R.A. Kaye, T.L. Khoo, T. Lauritsen, C.J. Lister, E.F. Moore, M.A. Riley, D. Seweryniak, I. Shestakova, G. Sletten, P.M. Walker, C. Wheldon, I. Wiedenhöver, O. Zeidan, Jing-Ye Zhang, Phys. Lett. B **560**, 24 (2003).
25. D.R. Jensen, J. Domscheit, G.B. Hagemann, M. Bergström, B. Herskind, B.S. Nielsen, G. Sletten, P.G. Varmette, S. Törmänen, H. Hübel, W.C. Ma, A. Bracco, F. Camera, F. Demaria, S. Frattini, B. Million, D. Napoli, A. Maj, B.M. Nyakó, D.T. Joss, M. Aiche, Eur. Phys. J. A **8**, 165 (2000).
26. K.A. Schmidt, M. Bergström, G.B. Hagemann, B. Herskind, G. Sletten, P.G. Varmette, J. Domscheit, H. Hübel, S.W. Ødegård, S. Frattini, A. Bracco, B. Million, M.P. Carpenter, R.V.F. Janssens, T.L. Khoo, T. Lauritsen, C.J. Lister, S. Siem, I. Wiedenhöver, D.J. Hartley, L.L. Riedinger, A. Maj, W.C. Ma, R. Terry, Eur. Phys. J. A **12**, 15 (2001).
27. W. Schmitz, C.X. Yang, H. Hübel, A.P. Byrne, R. Müsseler, N. Singh, K.H. Maier, A. Kuhnert, R. Wyss, Nucl. Phys. A **539**, 112 (1992).
28. R. Bengtsson, T. Bengtsson, M. Bergström, H. Ryde, G.B. Hagemann, Nucl. Phys. A **569**, 469 (1994).
29. T. Bengtsson, Nucl. Phys. A **496**, 56 (1989).
30. R. Bengtsson, W. Nazarewicz, Z. Phys. **334**, 269 (1989)
31. R. Bengtsson, H. Ryde, to be published.
32. P. Olivius, PhD Thesis, Lund Institute of Technology (2004).